DESIGN AND FIRST OPERATION OF AN ADVANCED ORC-CHP ARCHITECTURE

Sebastian Eyerer [1]*, Fabian Dawo [1], Maximilian Altnöder [1], Roland Windhager [1], Anne Niederdränk [1], Helge Esch [1], Stefan Ausfelder [1], Robin Konrad [1], Michael Höger [1], Christoph Wieland [1] and Hartmut Spliethoff [1,2]

[1] Institute for Energy Systems, Faculty of Mechanical Engineering, Technical University of Munich, Boltzmannstraße 15, 85748 Garching, Germany
sebastian.eyerer@tum.de, fabian.dawo@tum.de, maximilian.altnöder@tum.de, roland.windhager@tum.de, anne.niederdraenk@tum.de, helge.esch@tum.de, stefan.ausfelder@tum.de, robin.konrad@tum.de, michael.hoeger@tum.de, wieland@tum.de, spliethof@tum.de

[2] Bavarian Center for Applied Energy Research, Garching, Germany
Walther-Meißner-Str. 6, 85748 Garching, Germany
spliethof@tum.de

* Corresponding Author

ABSTRACT

Over the last years, the optimization of the Organic Rankine Cycle technology has been enforced. There are several approaches to increase the efficiency of ORC plants, including the ORC plant design, the working fluid selection, the part-load optimization together with combined heat and power (CHP) generation, as well as the optimization of the plant components. In order to contribute to these optimization measures, the design and first operation of an advanced ORC-CHP plant architecture optimized for geothermal applications, is presented in this study. This architecture extends the state of the art ORC by a two-stage expander with turbine bleeding and a regenerative direct contact preheater. The aim of this architecture is to increase the utilization of the heat source, the flexibility and the part-load efficiency of the plant. In order to evaluate the performance of this ORC-CHP concept, a test rig has been constructed. The test rig is heated with a 200 kW electrical resistance heater, which is controlled by pulse width modulation. As expander, a twin screw compressor is used, which operates in reverse mode and R1233zd(E) is applied as working fluid. Besides an in-depth description of the test rig, the system is analyzed in its complete operational range. Therefore, experiments are conducted with varying heat loads of the district heating network. With this, an operation strategy of the ORC system for the full operational range is derived.

1. INTRODUCTION

The aim to reduce CO_2 emissions leads to a growing importance of renewable sources and a strong focus on efficient heat and power production. Therefore, the energy system is faced with versatile challenges concerning the security of supply, economic benefit for the operators as well as the environmental impact. In order to deal with these challenges and to pave the way for better commercialization, future energy systems must feature a high level of flexibility to cover wide operating ranges. Against this background, the Organic Rankine Cycle (ORC) technology is promising due to its ability to convert low temperature heat i.e. waste heat (Pili *et al.*, 2017) or heat from renewable sources such as biomass (Preißinger *et al.*, 2012), solar (Li, 2015) or geothermal (Eyerer *et al.*, 2019c) to power. Especially for the geothermal application the part load performance and flexibility is a very important design aspect (Dawo *et al.*, 2019).

Within the last decades, the ORC technology has been established in commercial products and its advantages has been proven in operation. However, the continuous optimization of the technology is important in order to meet the challenges of the energy transition. Therefore, several optimization measures have been studied in literature with both, experimental and numerical investigations. The main optimization paths of the technology can be classified in five groups: advanced plant architecture (Lecompte *et al.*, 2015), part-load optimization and control (Hernandez *et al.*, 2015), modern working fluids (Eyerer *et al.*, 2019a), cogeneration (Wieland *et al.*, 2016), component optimization (Kang, 2016).

In the field of advanced plant architectures, Branchini *et al.* (2013) and Mago *et al.* (2008), investigated an ORC with turbine bleeding and a direct contact heat exchanger for regenerative preheating of the working fluid. Mago *et al.* (2008) concluded that this advanced architecture leads to an increase in thermal efficiency and a reduction of the irreversibility, although the performance is heavily depending on the applied working fluid. This regenerative ORC concept was also analyzed by Braimakis and Karellas (2018) as well as Meinel *et al.* (2014b). In their numerical study, Meinel *et al.* (2014b) compared the regenerative ORC with a standard ORC as well as with a recuperated ORC and additionally investigated the influence of different working fluids. They concluded that the regenerative ORC is beneficial for isentropic and wet fluids, while for dry fluids, the recuperation is more efficient. For the isentropic fluid R245fa, they reported a higher thermal efficiency of up to 2.25% of the regenerative ORC compared to the standard ORC and an increase of up to 1.22% compared to a recuperative ORC. In a follow up study, Meinel *et al.* (2014a) analyzed the effect of this more complex plant architecture on the levelized cost of electricity. They concluded that the increased equipment costs due to the additional components (second pump, direct contact heat exchanger) are compensated by the smaller heat exchanger area of the preheater. Together with the increased thermal efficiency, the levelized cost of electricity (LCOE) of the regenerative ORC using R245fa as working fluid is 7 % lower compared to standard ORC with 500 kW_{el} capacity. For the regenerative ORC, the increase in thermal efficiency is mainly caused by a reduction of the necessary heat for the cycle. Thus, the outlet temperature of the heat source is higher compared to the standard ORC. This higher temperature enables the further utilization of the heat source for combined heat and power production. Based on these considerations, Wieland *et al.* (2015) developed an ORC-CHP concept using a regenerative ORC in combination with a controllable preheater and flexible heat decoupling. This concept was patented and numerically investigated (Meinel *et al.*, 2016). Therefore, they compared the novel ORC-CHP concept with a standard ORC with parallel heat decoupling in heat-driven operation. They assumed a heat source temperature of 240 °C and used R1233zd(E) as working fluid. Their results revealed a 3.1% higher annual electricity generation for the novel ORC-CHP concept compared to the standard ORC with parallel heat decoupling. Besides the analysis of the regenerative ORC, Lecompte *et al.* (2015) made a literature review concerning ORC plant architectures and compared the standard ORC with a regenerative, a recuperative and a transcritical ORC as well as with an ORC with multiple pressure levels. Especially for complex architectures such as the regenerative ORC and multiple pressure levels, they reported a lack of experimental investigations.

The above-discussed literature shows the benefits of a regenerative ORC especially in combined heat and power operation. However, according to the authors' knowledge, such a two-stage ORC concept has not yet been investigated experimentally. Thus, the purpose of this publication is to analyze the advanced ORC-CHP concept with turbine bleeding, regenerative preheating and flexible heat decoupling in a test rig.

In order to meet this purpose, the basic functionality of the advanced ORC-CHP concept is described first. Then, the test rig is described in detail and the experimental methodology is introduced. Afterwards, the experimental results are presented and discussed. Finally, relevant conclusion are drawn.

2. SYSTEM DESCRIPTION AND FUNCTIONALITY

The basic layout of the ORC-CHP concept is depicted in Figure 1 for an arbitrary liquid heat source such as geothermal brine or heat transfer medium from solar thermal energy, biomass combustion or waste heat applications. The explanation of the layout starts with the heat source cycle, where the hot

fluid is directed to the evaporator (6). Depending on the heat demand in the district heating system (DHS) (15), the necessary heat source stream through the heat network exchanger (13) is controlled by valve (11). Only in cases in which the required supply temperature of the DHS cannot be ensured with the stream leaving the evaporator, valve (12) opens and a part of the initial hot heat source stream is appended in order to lift the temperature in front of the DHS heat exchanger (13). If the required heat demand of the DHS is satisfied, valve (11) directs the excess stream of the heat source to the low-pressure preheater (3) to be further cooled down.
In order to explain the operational strategy of the actual ORC loop, the two extreme load cases of the DHS demand as well as one intermediate load case are discussed in the following. Starting with zero heat demand in the DHS, valve (11) directs the total heat source stream to the low-pressure preheater (3). With this, the transferred heat in this exchanger is sufficient to preheat the ORC working fluid. Thus, the low-pressure pump (1) pressurizes the liquid condensate to an intermediate pressure level and valve (2) directs the working fluid to the low-pressure preheater (3), where it is preheated by cooling down the heat source. Depending on the size of the low-pressure preheater (3), it is even possible to partially evaporate the fluid. In order to ensure a saturated liquid state in the direct contact heat exchanger (4), valve (2) directs a small portion of the cold liquid fluid straight to the direct contact heat exchanger. The high-pressure pump (5) then pressurizes the preheated liquid fluid to high-pressure level and feeds the evaporator (6), where the fluid is further preheated to saturation, evaporated and slightly superheated. The resulting live vapor is then expanded in the expansion machine (7), which in turn drives the generator to produce electricity. The exhaust vapor leaving the expansion machine is desuperheated and condensed in the condenser (9) and fed into the receiver tank (10) for the low-pressure pump (1), where the cycle starts again.

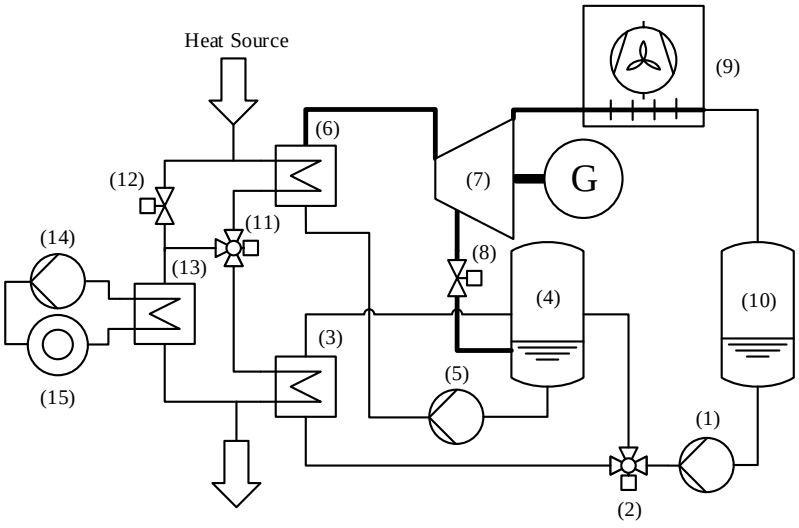

Figure 1: Plant architecture of the regenerative ORC-CHP concept

If the heat demand in the district heating system increases, valve (11) only directs a smaller share of the heat source stream to the low-pressure preheater (3) and hence the required preheating cannot necessarily be achieved in the low-pressure preheater. In this case, the branch of valve (2) towards the direct contact heat exchanger is completely closed. Furthermore, valve (8) opens and vapor at an intermediate pressure level is extracted from the expander in order to further preheat the fluid in the direct contact heat exchanger. The following process is analogous to the case above.
In the case of maximum heat demand in the DHS, the branch of valve (11) towards the low-pressure preheater is completely closed and the total heat source stream is directed to the DHS heat exchanger. In this case, the preheating of the working fluid needs to be solely covered by vapor extraction.
This description of the system functionality also indicates the operational range of the system. Starting with zero heat demand in the DHS, the ORC system can be operated at full load. With higher heat demand, the regenerative preheating is activated and the extraction flow rate increases with further rising DHS heat demand. With this vapor extraction, the power output of the system decreases while the thermal efficiency increases, as discussed in section 1.

3. EXPERIMENTAL FACILITY AND METHODOLOGY

3.1 ORC System and Control Options

An image of the test rig with all components is shown in Figure 2. Furthermore, Figure 3 depicts a simplified piping and instrumentation diagram (PID), in order to better understand the setup of the system. Within the PID the control strategy is also indicated by the dashed lines connecting the actuators with the respective sensors of the control loops. In this PID, only the components and sensors relevant for the experimental analysis of the present ORC-CHP architecture are included. This is also the reason, why the names of the respective components and sensors sometimes do not follow an ascending order.

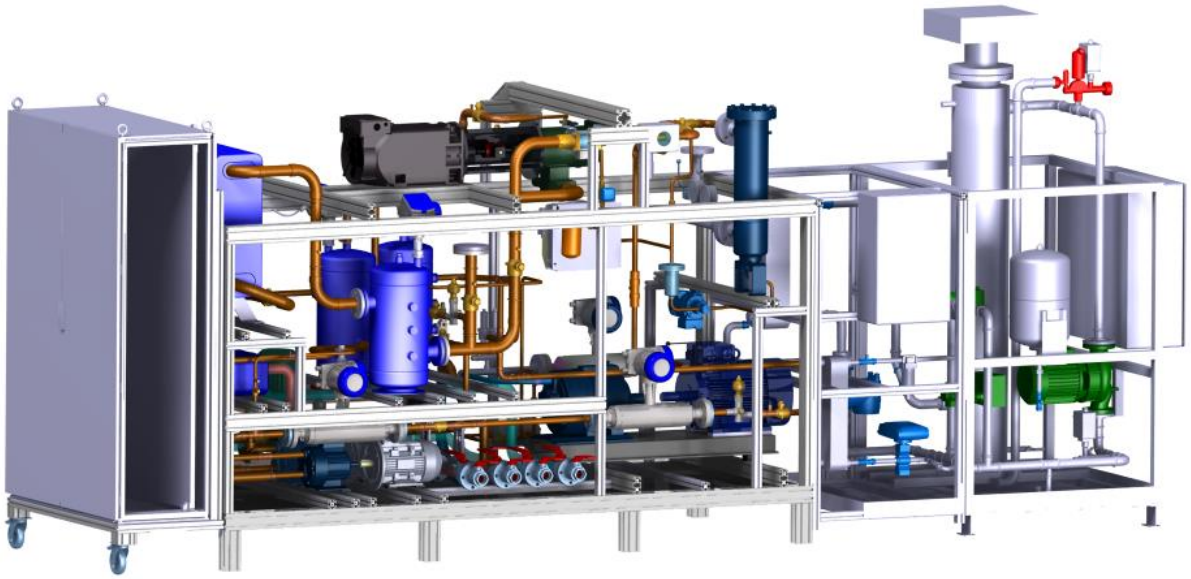

Figure 2: CAD image of the ORC-CHP test rig

The test rig consists of four different circuits: the heating circuit, the actual ORC circuit, and two cooling circuits: One for condensation and one for subcooling of the working fluid. In the following description of the test rig, the manufacturer and the name of the main components are included in brackets. In the heating circuit, water is used as heat carrier and a 200 kW electrical resistance heater is applied as the heat source. By pulse width modulation, the power of this heater can be adjusted in order to control the temperature at the inlet of the evaporator. This heating circuit is designed for a maximum temperature of 140 °C, which is a typical heat source temperature i.e. for geothermal applications. Besides the heat source temperature, also the flow rates in the heating circuit can be controlled using the rotational speed of the centrifugal heating circuit pump (Wilo IPn 40/160-2,2/2) and the valve position of V2, V3 and V4 (ESBE VLE 122) as manipulated variables. Hereby, the flow rates through the evaporator (Alfa Laval CBH112-52H-F), the low-pressure preheater (Alfa Laval CBH60-32H-F) and the evaporator bypass can be controlled individually. Compared to the plant architecture in Figure 1, there is no DHS connected to the test rig. Instead, the heat is directly recycled in order to reduce the power consumption of the resistance heater. For the experiments, the required DHS heat demand is then considered via an energy balance and the enthalpy streams flowing through the valves V3 and V4.

In the ORC circuit, two positive displacement pumps (Verder G10 EKCEHFEMC), connected in parallel, are used as low-pressure pumps. The rotational speed of these pumps can be adjusted in order to control the liquid level inside the direct contact heat exchanger. This direct contact heat exchanger is a 30 L pressure vessel from A-Cold. The temperature and thus the pressure inside this vessel is controlled by adjusting the positions of the valves V22, V23 (Danfoss ETS 100B) and V24 (Alco EX8-U21). Therefore, a twofold control strategy is implemented. For low DHS heat demands, no vapor is extracted from the expander as described above. Thus, the extraction valve V24 is closed and the temperature inside the direct contact heat exchanger is only controlled by V22 and V23. If the heat demand in the DHS increases to a certain point, the heat transferred in the low-pressure preheater is not

enough to maintain the setpoint temperature in the direct contact heat exchanger, even though V23 is completely open and V22 is completely closed. Then, the extraction valve V24 takes over the temperature control and opens the extraction port of the expander. This port is placed at 55% of the built-in volume ratio of the expander starting from the high-pressure side. This value was chosen since there was an appropriate position in the housing of the expander where the extraction port could be placed. Furthermore, preliminary simulations revealed that the optimal position for the extraction port is approximately in the middle of the built-in volume ratio. As expander, an open type twin-screw compressor (Bitzer OSN5361-K) with a built-in volume ratio of 3.1 is applied and operated in reverse. The extracted vapor from the expander is then introduced with a bubbler pipe below the liquid level, in order to enhance the heat transfer in the direct contact heat exchanger. This bubbler pipe has many small holes so that small vapor bubbles are formed which rise in the liquid column. By this means, an effective condensation of the extracted vapor and a good heat transfer with the liquid in the vessel can be achieved. Due to the liquid-vapor equilibrium inside the direct contact heat exchanger, saturated liquid fluid leaves the vessel towards the high-pressure pump, which is again a positive displacement pump (Verder G35 XKCGHFEYA). In order to prevent cavitation of this pump, a fraction of cold liquid is injected into the pipe in front of the high-pressure pump to slightly subcool the saturated liquid. Therefore, the position of valve V26 (Danfoss ETS 12.5) is adjusted so that the required net positive suction head (NPSH) of the high-pressure pump is maintained. The rotational speed of this pump is then adjusted in order to control the superheating of the live vapor at the expander inlet. Furthermore, the live vapor pressure is controlled by the rotational speed of the expander. Since the pressure controller also effects the superheating controller, both controllers have been designed with different time constants. Thus, the pressure controller is approximately one order of magnitude faster than the superheating controller.

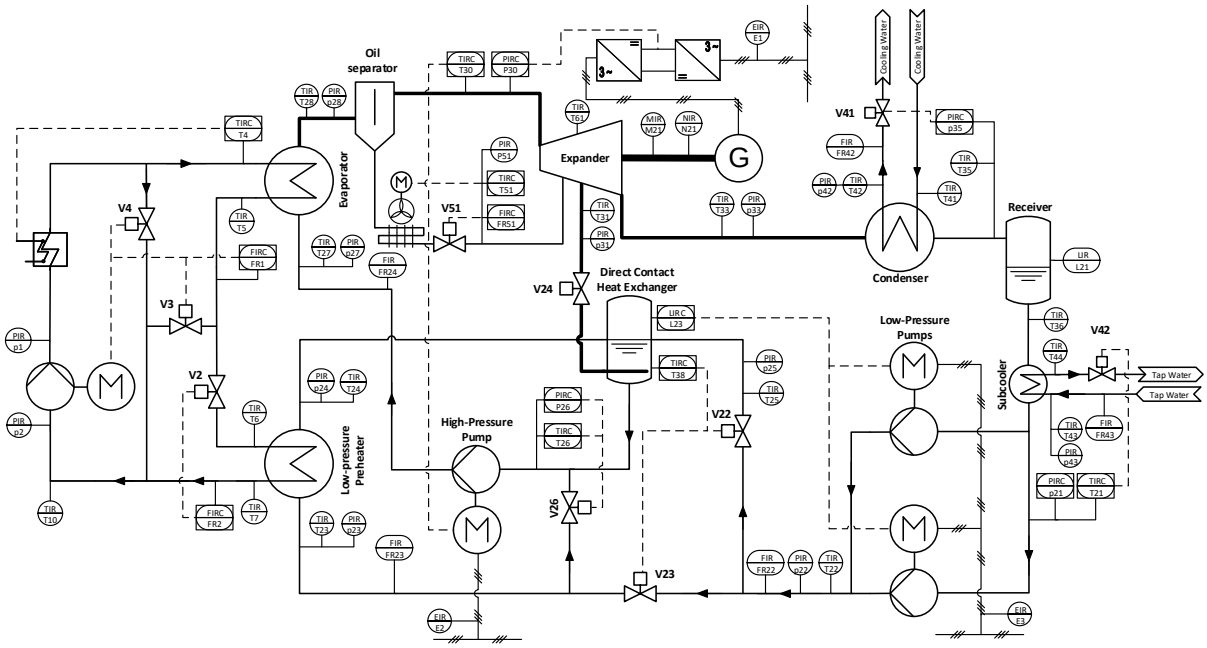

Figure 3: Simplified PID of the test rig with control loops

The heat sink of the test rig consists of two cooling circuits. In the first cooling circuit, cooling water is used as heat transfer medium flowing through a brazed plate condenser (Alfa Laval CB112-170H). Its flow rate is adjusted by V41 (ESBE VLA 325) in order to control the condensation pressure and thus the condensation temperature. The heat in this cooling circuit is then released to the atmosphere by a wet cooling tower outside of the lab. The condensate is subsequently fed into a 30 L liquid receiver. Similar to the direct contact heat exchanger, the fluid inside this receiver is saturated. In order to ensure the required NPSH of the low-pressure pumps, the second cooling circuit is used to further cool the liquid fluid in the subcooler heat exchanger (Alfa Laval CB60-60M-F). Therefore, valve V42 (ESBE VLE 122) adjusts the tap water flow to control the available NPSH in front of the low-pressure pumps.

Additionally to the above-presented circuits, the expander has to be lubricated. Therefore, the working fluid is mixed with refrigerant oil (Reniso Triton SE 220). During evaporation of the working fluid, the oil is dragged as a spray. These small oil droplets are separated from the live vapor within the oil separator (ESK Schulze BOS 2-54/42F). The degree of separation of this device is below unity. Thus, some oil remains in the live vapor and lubricates the rotors of the expander. However, the major part of the oil is separated and directed to the bearings for lubrication and cooling. Consequently, the oil temperature in front of the expander is controlled by an air-cooled heat exchanger. Furthermore, valve V51 controls the oil flow rate to the required value.
As indicated in Figure 3, the ORC system is fully instrumented with temperature and pressure sensors before and after each component, mass-flow sensors in each relevant branch as well as sensors for electrical power measurement. All the instrumentation and measurement ranges as well as the accuracy of each sensor are summarized in Table 1. Depending on the sensor type, the measurement accuracy is either constant or a linear function of the measured value (MV).

Table 1. Measuring range and accuracy of the relevant sensors

Measured parameter	Sensors	Measurement principle	Measurement range	Accuracy of measurement	Output signal
Pressure	p1, p2, p42, p43	Strain gauge	0 – 10 bar	±0.05 bar	4-20 mA
	p21 – p26, p31 – p35		0 – 16 bar	±0.08 bar	
	p30, p51		0 – 40 bar	±0.20 bar	
	p27, p28		0 – 60 bar	±0.30 bar	
Temperature	T27, T28	PT100 class A	-100 – 400 °C	±(0.002·MV+0.15 °C)	resistance
	all other	PT100 class AA	0 – 150 °C	±(0.0017·MV+0.1 °C)	
Mass flow	FR22 – FR24	Coriolis	0 – 1.5 kg/s	±(0.0015·MV+ 0.75 kg/s)	4-20 mA
Volume flow	FR1	Inductive	0 – 250 L/min	±0.005·MV + 0.03 L/min	4-20 mA
	FR2	Inductive	0 – 50 L/min	±0.004·MV + 0.01 L/min	
	FR42, FR43	Displacement	10 – 400 l/min	±12 L/min	
Tank level	L23	Radar	0 – 550 mm	±3 mm	4-20 mA
El. power	E1 – E3	El. power meter	0 – 40 kW	±0.01·MV	digital
Rotational speed	N21	Hall	0 – 7500 rpm	±15 rpm	4-20 mA

The process control system with all the above-discussed control loops as well as the data acquisition of all sensors is implemented in LabView. For the input/output (I/O) communication a real time system (NI cRIO 9067) together with several I/O modules for analogue and digital input and output signals is used. In order to obtain the measurement errors, the accuracy of the sensor and the data acquisition system need to be considered. Therefore, Table 2 shows the precision of the used I/O modules.

Table 2. Range and accuracy of the relevant I/O modules

I/O Module	Range	Module Accuracy	Connected sensors
NI 9208	-22 – 22 mA	$\pm(0.0076 \cdot MV + 9.08 \cdot 10^{-3}$ mA)	Pressure, flow rate, rotational speed, tank level
NI 9216	0 – 400 Ω	± (0.00007·MV + 0.1654 °C)	Temperature
NI 9425	0 – 24 V	± 36 W [a]	Power meter

[a] Maximum discretization error

3.2 Methodology of Experiments

For the evaluation of the proposed ORC-CHP architecture, in total 21 stationary operation points in full load and part load operation are investigated. During all experiments, the heat source temperature and heat source flow rate are controlled to constant values of 135 °C and 0.6 kg/s, respectively. The same is done for the heat sink, where the condensation temperature is controlled to 40 °C. Furthermore, the setpoint of the temperature inside the direct contact heat exchanger T38 is 65 °C and the superheating at the expander inlet is controlled to a constant value of 5 K. In order to operate the ORC-CHP system in different load cases, the heat load of the DHS is varied. Starting from zero heat load, the valve V3 is opened stepwise in order to increase the DHS heat load. The temperature control in the direct contact heat exchanger is then carried out as described above. For lower heat demands, the transferred heat in the low-pressure preheater is sufficient for keeping the temperature in the direct contact heat exchanger at its setpoint of 65 °C. For increasing DHS heat load, V24 opens the extraction port of the expander and the regenerative preheating is activated to control T38. As long as V24 is closed, the live vapor pressure

is kept constant at its optimal value of 8.5 bar_{abs}. However, with further increasing of the DHS heat demand, the live vapor pressure has to be increased in order to keep the temperature in the direct contact heat exchanger at its setpoint and to ensure a DHS supply temperature of 80 °C. To calculate the DHS heat demand, a return temperature of 50 °C and a pinch point temperature difference of the heat network exchanger (component (13) in Figure 1) of 5 K is assumed. With this, the heat source stream through V3 can be virtually cooled down to 55 °C.

For all operating points, stationary conditions are maintained for at least 10 min. For data evaluation, a measurement value is acquired for each sensor every second. In order to post-process these raw data, an algorithm has been developed to detect the best stationary points. For a detailed description of this algorithm, reference is made to Eyerer *et al.* (2019b). Using these steady-state operation conditions, further relevant properties such as enthalpy, entropy and density are calculated with Refprop 10.0 (Lemmon *et al.*, 2018). The measured values, together with the calculated fluid properties, are used to obtain characteristic process parameters such as efficiencies. Based on the accuracies of the sensors and the data acquisition system (cf. Tables 1 and 2), the measurement errors of each value are calculated using the Gaussian law of error propagation. For a description of the procedure of uncertainty analysis, reference is made to Eyerer *et al.* (2019a). The resulting uncertainties are highlighted in the corresponding figures in the next section with error bars adjacent to the measured mean value.

4. RESULTS AND DISCUSSION

Following the experimental procedure described above, the complete operational range in terms of electrical and thermal power output is depicted in Figure 4 (a). There, the net power output is defined as the difference between the power output of the generator and the power consumption of the low-pressure and high-pressure pumps. The maximum net power output of 6.92 kW_{el} is reached for zero heat demand, while the minimum power output is 1.06 kW_{el}. This corresponds to a minimal electrical load of 15.3 % of the nominal load. With this, the operational range of the ORC in terms of power output is very high. The minimum power output is reached for the maximum DHS heat load of 130.72 kW_{th}. The limit for this minimum load is the lower bound of the rotational speed of the expander. According to Wieland *et al.* (2016), the CHP coefficient, defined as the ratio of electrical and thermal power output, is a good measure for the flexibility of a CHP system. In the case of the present ORC-CHP architecture, this coefficient ranges from infinity (with zero heat demand) to 0.008 at the point of maximum DHS heat demand. With this high operational range, the system is very flexible in terms of electricity and heat production.

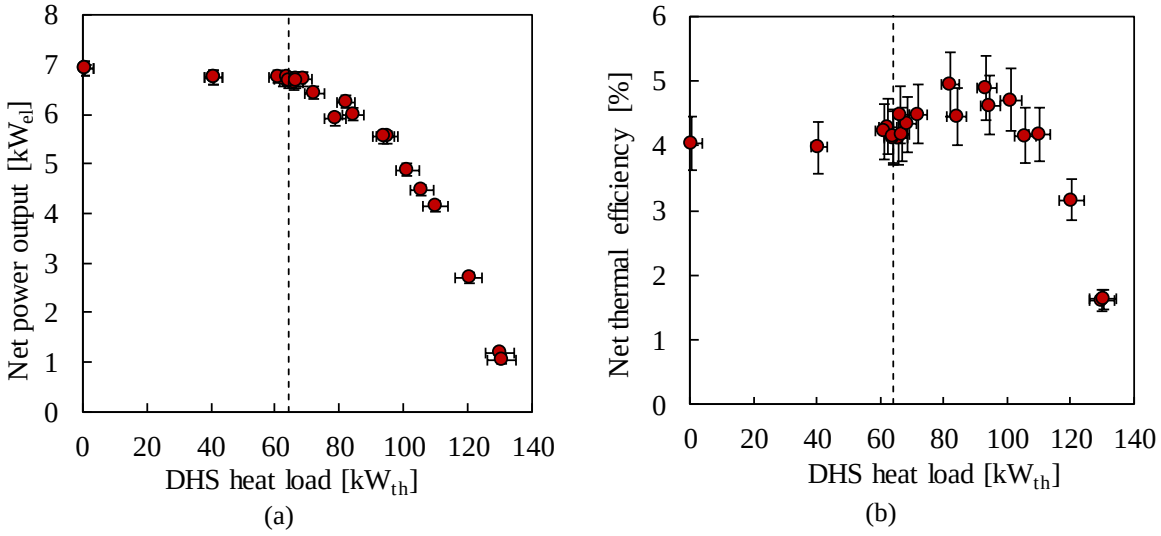

Figure 4: Power output (a) and thermal efficiency (b) of the ORC-CHP system for different DHS heat loads

When looking at Figure 4 (a), the operational range of the system can be divided into two regions. Their border is highlighted by the vertical dashed line in Figure 4 (a) and all following graphs. For heat loads below this border, the preheating to the required temperature level in the direct contact heat exchanger

is solely done by the low-pressure preheater. Due to the much higher heat capacity flow of the heating water compared to the working fluid stream in the low-pressure preheater, the DHS heat load can be increased without affecting the power output of the ORC. When the DHS heat load exceeds the dashed line, the vapor extraction is activated. This can be seen in Figure 5 (a), where the extraction ratio is depicted over the DHS heat load. There, the extraction ratio is defined as the ratio of the extracted mass flow rate and the mass flow rate entering the expander. Depending on the heat load, the extraction ratio rises to 13.5%. As mentioned above, the live vapor pressure needs to be increased in order to keep the temperature inside the direct contact heat exchanger at its setpoint of 65 °C. This increase in live vapor pressure is shown in Figure 5 (b). Both effects, the increased extraction ratio and the reduced live vapor mass flow rate caused by the increased live vapor pressure, lead to a reduction of the electrical power output, which can be seen in Figure 4 (a) in the region on the right side of the dashed line.
On the contrary, the thermal efficiency, defined as the ratio between electrical power output and transferred heat to the working fluid, increases due to the regenerative preheating and the increased live vapor pressure, which can be seen in Figure 4 (b). This shows that the thermal efficiency of the system enhances during part load operation. The maximum thermal efficiency of 4.95 % is reached for a DHS heat demand of 82.1 kW_{th}. For further increasing heat demand, the thermal efficiency drops (cf. Figure 4 (b)). This can be explained by increasing losses within the expander and thus a reduction of the isentropic efficiency. Due to the increased live vapor pressure, the pressure ratio over the expander increases and the loss mechanism of under expansion becomes more important. Furthermore, higher live vapor pressures are achieved by reducing the rotational speed of the expander. With this internal leakage typically increases. Thermal efficiencies in the range between 4 – 5 % are quite low compared to other experimental investigations. The present test rig, however, features a high modularity in order to evaluate different plant architectures while using the same components. Thus, it is not designed for maximum efficiency.

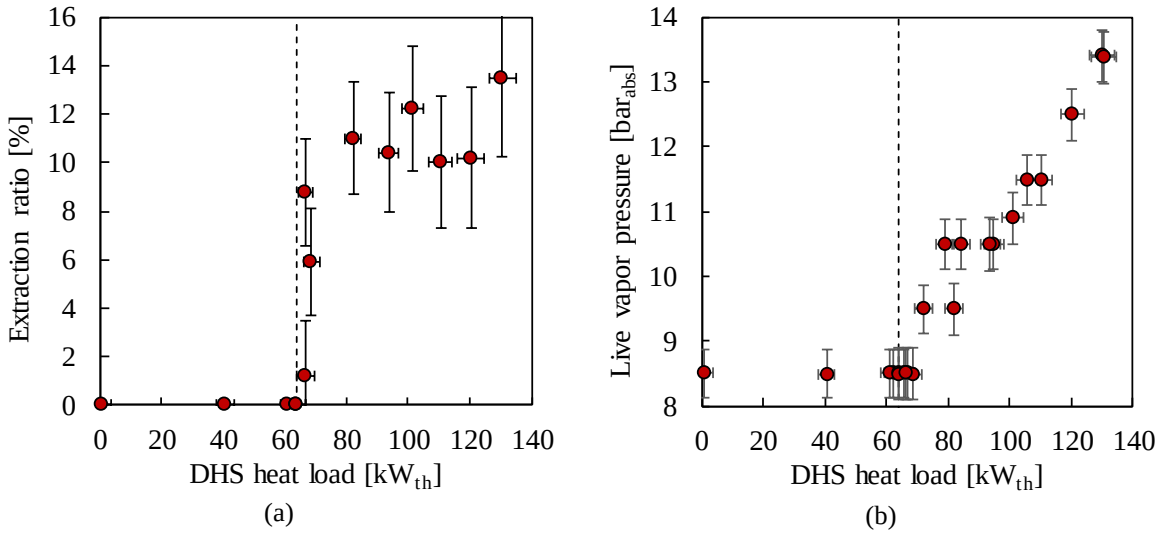

Figure 5: Extraction ratio (a) and live vapor pressure (b) of the ORC-CHP system for different DHS heat loads

5. CONCLUSIONS AND OUTLOOK

In this paper, the design and the first operation of an advanced ORC-CHP architecture are presented. This ORC-CHP concept features regenerative preheating of the working fluid through extraction of partially expanded vapor from the expander. Furthermore, a low-pressure preheater is used to provide flexibility to a changing load of the district heating system (DHS). The functionality of this architecture has been explained and the developed test rig has been introduced with an in-depth description of the control strategy. Based on the experimental analysis of this architecture, the following conclusions can be drawn:

- The ORC-CHP architecture features a high operational range down to a minimum load of 15.3 % of the nominal power output.

- The architecture has a wide range of possible CHP coefficients, ranging from infinity (i.e., without thermal power withdrawn) to 0.008. With this high operational range, the system is very flexible in terms of electricity and heat production.
- Due to the regenerative preheating and operational strategy of the system, the thermal efficiency increases during part-load operation.

In order to evaluate the presented ORC-CHP architecture in more detail, further experiments will be conducted in the future. First, the effects of the vapor extraction on the expansion process and the isentropic efficiency will be analyzed. Then, the novel concept will be compared with state-of-the-art ORC-CHP concepts such as parallel or serial heat decoupling. For a fair comparison of all these CHP architectures, the test rig is designed modular. Thus, the same equipment, such as heat exchangers, expander and feed-pumps, is used for the experiments. Based on this comparison, the benefits of the presented architecture can be evaluated for several applications such as geothermal or waste heat recovery. Besides the performance evaluation of the architecture, also the influence of the DHS generation in terms of supply and return temperature will be investigated.

ACKNOWLEDGEMENT

Funding from the Bavarian State Ministry of Education, Science and the Arts in the framework of the project Geothermal-Alliance Bavaria is gratefully acknowledged.

REFERENCES

Braimakis, K. and Karellas, S., 2018, Energetic optimization of regenerative Organic Rankine Cycle (ORC) configurations, *Energy Convers. Manag*., Vol. 159, pp. 353–370.

Branchini, L., Pascale, A. de and Peretto, A., 2013, Systematic Comparison of ORC Configurations by Means of Comprehensive Performance Indexes, *Appl. Therm. Eng*., Vol. 61 No. 2, pp. 129–140.

Dawo, F., Wieland, C. and Spliethoff, H., 2019, "Kalina power plant part load modeling. Comparison of different approaches to model part load behavior and validation on real operating data", *Energy*, Vol. 174, pp. 625–637.

Eyerer, S., Dawo, F., Kaindl, J., Wieland, C. and Spliethoff, H., 2019a, Experimental investigation of modern ORC working fluids R1224yd(Z) and R1233zd(E) as replacements for R245fa, *Appl. Energy*, Vol. 240, pp. 946–963.

Eyerer, S., Dawo, F., Pili, R., Niederdränk, A., Windhager, R., Wieland, C. and Spliethoff, H., 2019b, Advanced Injection Cooling Concept for Organic Rankine Cycles, in *32nd International Conference on Efficiency, Cost, Optimization, Simulation and Environmental Impact of Energy Systems*, Wroclaw, Poland, 23-28 June 2019.

Eyerer, S., Schifflechner, C., Hofbauer, S., Bauer, W., Wieland, C. and Spliethoff, H., 2019c , Combined heat and power from hydrothermal geothermal resources in Germany: An assessment of the potential, submitted to *Renew. Sust. Energ. Rev*.

Hernandez, A., Desideri, A., Ionescu, C., Quoilin, S., Lemort, V. and Keyser, R. de, 2015, Towards the Optimal Operation of an Organic Rankine Cycle Unit by Means of Model Predivtive Control, in *3rd International Seminar on ORC Power Systems*, Belgium, Brussels, 12-14 October.

Kang, S.H., 2016, Design and Preliminary Tests of ORC (Organic Rankine Cycle) with Two-Stage Radial Turbine, *Energy*, Vol. 96, pp. 142–154.

Lecompte, S., Huisseune, H., Broek, M. van den, Vanslambrouck, B. and Paepe, M. de 2015, Review of Organic Rankine Cycle (ORC) Architectures for Waste Heat Recovery, *Renew. Sust. Energ. Rev*, Vol. 47, pp. 448–461.

Lemmon, E.W., Huber, M.L. and McLinden, M.O., 2018, REFPROP Reference Fluid Thermodynamic and Transport Properties. NIST Standard Reference Database 23, Version 10.0.

Li, J., 2015, *Structural Opimization and Experimental Investigation of the Organic Rankine Cycle for Solar Thermal Power Generation*, Springer-Verlag Berlin Heidelberg.

Mago, P.J., Chamra, L.M., Srinivasan, K. and Somayaji, C., 2008, An Examination of Regenerative Organic Rankine Cycles Using Dry Fluids, *Appl. Therm. Eng*., Vol. 28, pp. 998–1007.

Meinel, D., Braimakis, K., Wieland, C., Karellas, S. and Spliethoff, H., 2016, Flexible Two-Stage Turbine Bleeding Organic Rankine Cycles (ORCs) for Combined Heat and Power Applications, in *29th International Conference on Efficiency, Cost, Optimization, Simulation and Environmental Impact of Energy Systems*, Slovenia, Portoroz, 19-23 June 2016, pp. 1–22.

Meinel, D., Wieland, C. and Spliethoff, H., 2014a, Economic Comparison of ORC (Organic Rankine Cycle) Processes at Different Scales, *Energy*, Vol. 74, pp. 694–706.

Meinel, D., Wieland, C. and Spliethoff, H., 2014b, Effect and Comparison of Different Working Fluids on a Two-Stage Organic Rankine Cycle (ORC) Concept, *Appl. Therm. Eng.*, Vol. 63, pp. 246–253.

Pili, R., Romagnoli, A., Spliethoff, H. and Wieland, C., 2017, Techno-Economic Analysis of Waste Heat Recovery with ORC from Fluctuating Industrial Sources, *Energy Procedia*, Vol. 129, pp. 503–510.

Preißinger, M., Heberle, F. and Brüggemann, D., 2012, Thermodynamic Analysis of Double-Stage Biomass Fired Organic Rankine Cycle for Micro-Cogeneration, *Int. J. Energy Res.*, Vol. 36 No. 8, pp. 944–952.

Wieland, C., Meinel, D., Eyerer, S. and Spliethoff, H., 2016, Innovative CHP Concept for ORC and its Benefit Compared to Conventional Concepts, *Appl. Energy*, Vol. 183, pp. 478–490.

Wieland, C., Meinel, D. and Spliethoff, H., 2015, Energiewandler zur Wandlung von Wärmeenergie in mechanische Energie No. DE 10 2014 000 308 B3.